Microfluid Nanofluid
DOI 10.1007/s10404-012-1007-6

RESEARCH PAPER

Centrifugo-magnetophoretic particle separation

Daniel Kirby · Jonathan Siegrist · Gregor Kijanka · Laëtitia Zavattoni · Orla Sheils · John O'Leary · Robert Burger · Jens Ducrée

Received: 13 February 2012 / Accepted: 14 May 2012

Abstract There has been a recent surge of research output on magnetophoretic lab-on-a-chip systems due to their prospective use in a range of applications in the life sciences and clinical diagnostics. Manifold applications for batch-mode or continuous-flow magnetophoretic separations of cells, proteins, and nucleic acids are found in bioanalytics, cell biology, and clinical diagnostics. To ensure stable hydrodynamic conditions and thus reproducible separation, state-of-the-art magnetophoretic lab-on-a-chip systems have been based on pressure-driven flow (Gijs in Microfluid Nanofluid 1:22–40, 2004; Pamme and Manz in Anal Chem 76:7250–7256, 2004; Pamme in Lab Chip 7:1644–1659, 2007; Karle et al. in Lab Chip 10:3284–3290, 2010), which involves rather bulky and costly instrumentation. In a flow-based system, suspended particles are following the liquid phase as a result of the Stokes drag, thus being fully exposed to divergent flow lines around obstacles and pump-induced pressure fluctuations. To eventually achieve more stable hydrodynamic conditions, improved control of magnetic particles, a more compact instrumentation footprint, and integration of high-performance upstream sample preparation, this work introduces a novel two-dimensional particle separation principle by combining magnetic deflection with centrifugal sedimentation in a stopped-flow mode (i.e., mere particle sedimentation). The experimental parameters governing our centrifugo-magnetophoretic system are the strength and orientation of the co-rotating magnetic field, the rotationally induced centrifugal field, and the size-dependent Stokes drag of the various particles with respect to the (residual) liquid phase. In this work, the following set of basic functional modes is demonstrated as proof-of-concept: separation of magnetic from non-magnetic particles, routing of magnetic particles based on control of the spin speed, and size separation of various magnetic particles. Finally, a biomimetic application involving the separation of particles representing healthy cells from a very small concentration of magnetic particles of a similar size, mass and magnetization as a immuno-magnetically tagged target cell, for instance mimicking a circulating tumor cell.

Keywords Centrifugal · Microfluidic · Magnetophoresis · Separation · Particles

1 Introduction

The isolation and identification of unique biological cells of interest from a large population of background cells remain a challenge in biomedical diagnostics and analysis (Gijs 2004; Pamme and Manz 2004; Pamme 2007; Pappas and Wang 2007). For example, the capture and isolation of rare bioparticles such as circulating tumor cells (CTCs) or septic bacteria, which may only be present in concentrations as low as 1 cell/mL of blood in an abundant background of other blood cells, bear an obvious application potential towards cancer screening and molecular diagnostics (Pappas and Wang 2007; Siegrist et al. 2009). While larger, automated systems, such as fluorescence- and magnetically assisted cell sorters (FACS and MACS,

D. Kirby (✉) · J. Siegrist · G. Kijanka · L. Zavattoni · R. Burger · J. Ducrée
Biomedical Diagnostics Institute,
National Centre for Sensor Research, School of Physical Sciences, Dublin City University, Dublin 9, Ireland
e-mail: daniel.kirby4@mail.dcu.ie

J. Ducrée
e-mail: jens.ducree@dcu.ie

O. Sheils · J. O'Leary
Department of Pathology, Trinity College, Dublin, Ireland

Published online: 08 July 2012

respectively), have been successful, their associated instrumentation and operation prove to be bulky, complex, and expensive (Pappas and Wang 2007).

Thus, the development of smaller-scale, microfluidic cell capture and isolation systems remains of high interest. Such systems would benefit from the commonly quoted advantages of microfluidics (e.g., high amenability to automation, process integration, multiplexing and parallelization, substantially reduced sample and reagent volumes, smaller instrument footprint, portability, low costs of ownership) while possibly gaining additional functionality over current mesofluidic systems (Beebe et al. 2002; Manz et al. 1990). However, proof-of-concept of such a system will only transfer into useful applications, if it can be integrated with upstream sample preparation (Haeberle et al. 2006) to form a full-fledged sample-to-answer technology. In the case of rare cell detection from whole blood, the platform utilized must also be able to process and handle the comparatively large blood-sample volumes in a low-loss fashion to obtain statistically representative counts of these bioparticles (Siegrist et al. 2009).

A common, general method for biological separation is the linking of analytes with particles/beads, followed by the subsequent control and separation. This continues to be a feasible approach to the problem, and has already found widespread commercial applications using magnetic particles (Gijs 2004; Pappas and Wang 2007; ThermoScientific KingFisher; Veridex). Smaller-scale systems have also been developed, including microfluidic continuous-flow and magnetophoretic systems (Gijs 2004; Pamme and Manz 2004; Pamme 2006; Pamme and Wilhelm 2006). To the best of the authors' knowledge, all continuous, microfluidic separation systems shown to date have been flow-based, pressure-driven systems. However, such implementations exhibit inherent disadvantages. Initial particle focusing is an issue, as the microparticles tend to follow divergent flow lines to compromise resolution. Moreover, pressure-driven systems, while providing good control at larger flow rates, tend to be difficult to manage at low flow rates, which are required for microparticle control and focusing (Ducrée et al. 2007; Gorkin et al. 2010; Madou 2002; Madou et al. 2006).

In an effort to overcome these disadvantages, this work adapts a magnetophoretic system onto a rotational lab-on-a-disc platform operating in stopped-flow mode. The centrifugal, artificial gravity force propels particles through a stagnant carrier fluid and separates/routes them according to their density, size, and magnetic properties in the presence of a co-rotating, permanent magnet polarized in a direction perpendicular to the centrifugal force. Apart from the elimination of (divergent) flow lines, obvious advantages are gained with the centrifugal system as compared to common pressure-driven schemes, including the simple, cost-efficient, low-maintenance instrumental setup ("CD player"), the ease-of-handling of the disc-shaped substrates ("CDs") that do not require tubing interconnects, and the freely programmable and inertially stabilized, jitter-free centrifugal actuation mechanism that features a large force range and a rotationally symmetric field for facile parallelization (Ducrée et al. 2007; Gorkin et al. 2010; Madou et al. 2006; Burger and Ducrée 2012).

1.1 System concept, design, and advantages

In this work, a magnetophoretic system inspired by the concepts of Pamme and Manz (2004) was for the first time adapted onto a centrifugal microfluidic platform towards cell separation applications. The device works by centrifugally sedimenting particles in a stagnant carrier fluid through a magnetic field generated by disc based permanent magnets (Fig. 1). The novel, two-dimensional, centrifugo-magnetophoretic system is governed by the interplay of several experimental control parameters and forces as follows: rotational spin speed (controls centrifugal field), particle size and viscosity of the carrier fluid (affects Stokes drag), particle density (impacts sedimentation rate), and the geometry of the separation chamber (controls, for instance, particle residence time and magnetic field distribution). Moreover, the strength, position, and orientation of the co-rotating permanent magnet can also be customized.

The entire system (Fig. 2) is first primed with liquid. Next, a particle suspension is introduced to the loading chamber. After mounting of the on-chip permanent magnet, the hybrid, microfluidic disc is placed on a spin-stand motor and rotated at various speeds to centrifugally sediment and separate/route the particles. The particles first enter the focusing channel where they are aligned along the wall distant to the magnet (Fig. 1). Upon leaving the focusing channel, magnetic particles are immediately deflected towards the permanent magnet near the opposite sidewall of the separation chamber. Depending on the spin speed and their size, the particles either arrive in the capture notch A (towards low RPM) or the collection reservoir C (towards high RPM). In contrast, all non-magnetic particles sediment on straight, radial trajectories through the separation chamber into reservoir B.

It is worth emphasizing again that sedimentation occurs without flow; particles merely sediment through the stationary carrier fluid; therefore, eliminating impairment of the separation resolution caused by divergent flow lines and hydrodynamic instabilities. Thus, if these magnetic and non-magnetic particles are mixed and introduced simultaneously, they can easily be spatially separated, even under low hydrodynamic or mechanical stress (e.g., compared to just holding a permanent magnet against the outer wall of the vessel).

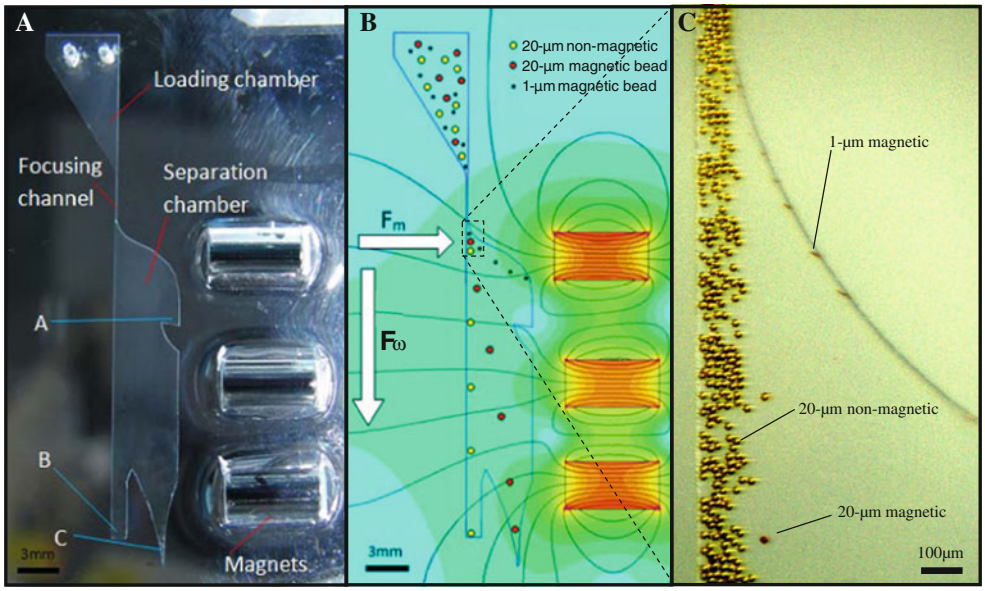

Fig. 1 **a** Photograph of a single centrifugo-magnetophoretic separation device on the disc with relevant features labeled. **b** Schematic and magnetic model showing the separation forces present in the system with calculated trajectories and destinations of three different particles. The centrifugal force f_ω and the magnetic force f_m are also displayed, with magnetic field intensity being represented by a *color gradient*. Magnetic modeling was done with the program "FEMM-finite element method magnetics". The Coriolis force is not shown but it will act opposite to the direction of rotation (i.e., pointing away from the magnets). **c** Image of three-way separation of beads at the opening of the separation chamber as outlined in the schematic. 1-μm particles have formed "trains" along the *field lines* and are, therefore, visible as *long streaks*, not individual spheres

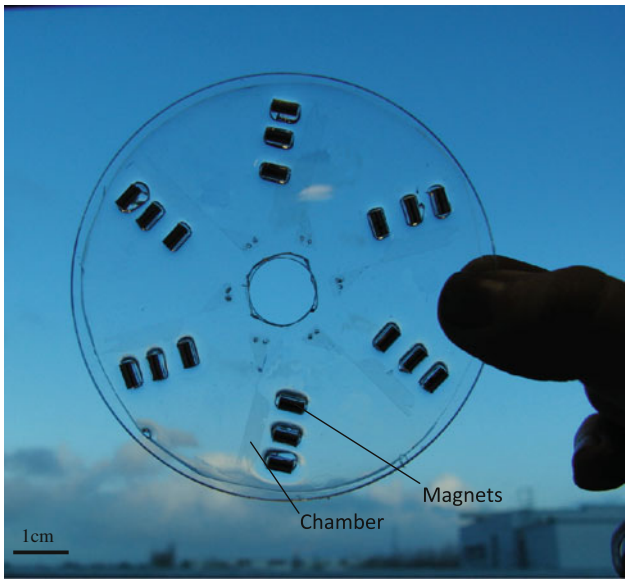

Fig. 2 Photograph of entire disk, showing six microfluidic chambers with three magnets parallel to each chamber. The magnified views of the individual chambers can be seen in Fig. 1

Within the wide spectrum of possible system designs and operational parameters, this proof-of-concept paper reports on a specific geometrical layout that was chosen to display several basic functional modes of the centrifugal magnetophoretic system. In this work, silicone discs are fabricated and tested to first show separation of magnetic from non-magnetic particles. Next, separation of different sizes of magnetic particles is shown, followed by routing of a fixed type of magnetic particle to a designated location controlled by the rotational spin speed. Finally, we present a threefold differential separation of a mixture of non-magnetic particles and magnetic particles of different sizes. This particle separation may be regarded as biomimetic of an actual sample of untagged cells, magnetically tagged cells and excess tagging particles.

2 Materials and methods

2.1 Device fabrication

The microfluidic devices were designed in AutoCAD (Autodesk, Inc., CA, USA) and fabricated out of polydimethylsiloxane (PDMS) (Sylgard 184, Dow Corning; #101697, Farnell, UK) using standard SU-8 soft-lithography processes (Xia and Whitesides 1998; Steigert et al. 2007a, b). A two-level, SU-8 mold was created on a bare, 4″ Si wafer by first spinning on SU-8 3050 (Microchem, MA, USA) to a thickness of 100 μm; this first layer formed the focusing channels and separation chambers (Fig. 2). The second SU-8 layer was spun on to a thickness of 150 μm and formed the loading chambers. Baking, UV exposure, and developing steps were performed separately for each layer according to the manufacturer's

recommendations. Note that each disk contains six identical separation structures.

After creation of the SU-8 mold, it was cleaned using UV/ozone for 5 min and then silanized using octadecyltrichlorosilane (#O5877, Sigma-Aldrich, IE) vapors for at least 4 h to promote PDMS release. To prepare the PDMS, Sylgard 184 curing agent and base were mixed in a ratio of 1:5 by weight, degassed, poured over the SU-8 mold, degassed again until all bubbles were eliminated, and then cured in an oven at 70 °C for 1 h. The PDMS part was removed from the mold, and holes, including the center hole, loading holes, and permanent magnet holes, were punched and cut out from the disc manually.

Next, stock 2-mm thick polymethylmethacrylate (PMMA) (#824-632, Radionics, IE) was laser cut into a standard CD format (12-cm diameter) and cleaned using isopropanol and DI water. Sylgard 184 curing agent and base, mixed this time in a mass ratio of 1:20, was mixed, degassed, and spun onto the PMMA disc at 1,500 revolutions-per-minute (RPM). The PDMS-coated disc was then cured in an oven at 70 °C for 1 h. Finally, the PDMS microfluidic device, with pre-cut holes, was manually aligned to the PDMS-coated PMMA base. The PDMS-to-PDMS bond was enabled by the mismatch in the concentrations of the curing agent (Thorsen et al. 2002), thus forming a practically irreversible bond between the PDMS layers. Adhesion between the spun-on PDMS and clean PMMA disc was completely leak-proof at the spin speeds used in these experiments.

2.2 Spin-stand instrument

To run the separation experiments, a servo-motor coupled to a stroboscopic visualization system similar to that already described in the literature (Grumann et al. 2005) was used for particle flow and tracking during rotation. A servo-motor (4490 series, Faulhaber, DE) was mounted to a framed support, and a custom chuck was machined for securely attaching standard discs to the servo-motor shaft. A CCD camera (Sensicam series, PCO, DE) was placed directly above the motor, and a combination of optical components (Navitar, NY, USA) and controls for particle visualization were attached to the camera to obtain a microscopic image; the optical setup also included a motorized zoom and focus to allow for multi-scale imaging of features on the microfluidic device. A linear drive was used to radially position the camera along the disc.

The camera was triggered to capture one frame per rotation, such that a movie composed of a sequence of still images taken at the same location on the disc could be acquired. A custom control box was fabricated to handle triggering between the motor, camera, and stroboscopic illumination system; the trigger box also served to control the circumferential location along the disc for image acquisition. The combined action of the linear camera drive and the trigger box provided full control to select the desired sector of the disc to be investigated and imaged. The stroboscopic system (Drelloscop 3244, Drello, DE) utilized a liquid light-conductor for illumination and was mounted above the disc and to the side of the camera. A desktop PC (Dell, US) was used to control the spin speed and sequences of the motor as well as for monitoring and image acquisition. The custom spin-stand instrument allowed for real-time movement and magnification, such that the flow of particles through the microfluidic device could be tracked. The optical clarity of the PDMS and PMMA device components, the bright stroboscopic illumination as well as coloring of the particles (Sect. 2.3) provided adequate contrast for visualization.

2.3 Particle separation experimental materials

Various types of particles were sourced for characterizing the centrifugal-based magnetophoretic system. The particles used included polystyrene particles ($d = 20.0$ μm; ~ 1.1 g cm^{-3}; #PS, MicroParticles, GmbH, DE), and iron-core, paramagnetic polystyrene particles of two different sizes ($d = 1.43$ and 18.8 μm; ~ 1.7 g cm^{-3}; #PS-MAG-S1792, #PS-MAG-S1985, and #PS-MAG-S1986, MicroParticles, GmbH, DE). The polystyrene particles were yellow and the magnetic particles were red; this allowed for easy visualization and differentiation on the spin-stand instrument and under the bright-light microscope. Particle sizes will be referred to as 20 μm (magnetic and non-magnetic), and 1 μm (magnetic) for convenience.

All particles arrived as either 5 or 10 % w/v solutions. After vortexing and/or sonication to homogenize the suspensions, dilutions of each particle type were made through a 1:10 ratio of particles to medium. The dilution medium consisted of phosphate buffered saline (PBS) with 0.1 % BSA. All particle mixtures were vortexed briefly before introduction to the disc.

2.4 Biomimetic separation experimental materials

For the biomimetic cell separation experiments, red, 20-μm magnetic particles were used to mimic cells of a similar size, mass and iron content which are coated with several hundred biofunctionalized 1-μm magnetic beads. Background, untagged blood cells were represented by 20-μm polystyrene particles as they were of a similar mass as blood cells and exhibit a different color to the magnetic particles. Finally, a real-world analytical sample would exhibit excess tagging particles, in this case 1.43 μm, magnetic iron cored polystyrene particles. These were also included in the sample to give a more realistic biomimetic

Table 1 Statistical data from five runs of 3-way particle separation

Capture area	20 μm non-magnetic	20 μm magnetic	1 μm magnetic
A	3 (0.02 %)	0 (0 %)	7.1×10^5 (100 %)
B	16,344 (99.93 %)	1.4 (3.7 %)	0 (0 %)
C	9 (0.05 %)	36 (96.3 %)	0 (0 %)

blood sample of 20-μm polystyrene beads, 20-μm iron cored polystyrene beads and 1-μm iron cored magnetic beads. This sample was then processed through the centrifugo-magnetophoretic system, and 3-way separation was observed as discussed in Sect. 3.2 (Table 1).

2.5 Experimental protocol and data analysis

After assembly and fabrication (Sect. 2.1), the microfluidic disc (Fig. 2) was primed with an excess (50 μL) of solution using degas-driven flow (Hosokawa et al. 2004) and then placed onto the spin-stand instrument. Nickel-plated, rod-shaped permanent magnets made of NdFeB (3 mm diameter, 6 mm long) (S-04-10-AN, SuperMagnete, DE) were mounted on the disc. Next, 2-μL aliquots of the various microparticle mixtures were placed in the loading chamber and then centrifugally sedimented through the system; spin speeds in the range of 225 RPM to 750 RPM were evaluated. A spin speed of 420 RPM was found to feature optimum separation of particles. The trajectories of the deflected particles were monitored using the stroboscopic imaging system described above and total number of particles trapped in each area was calculated using the theory of random loose packing (Silbert 2010) where the captured number of particles was large, and counted under an optical microscope where the number was small (roughly <20) and easily visible.

Particle deflection/separation was quantified by calculating the percentage of particles that ended up in each of the three chambers with the 1-μm magnetic beads in chamber A, the 20-μm non-magnetic beads in chamber B, and the 20-μm magnetic beads in chamber C (Fig. 3).

2.6 Magnetic modeling and measurements

To initially optimize the position and properties of the on-disc permanent magnet, we simulated the magnetic fields for various types and positions of permanent magnets (Fig. 1b) with the software package FEMM (Finite Element Method Magnetics (FEMM)). It was found that magnets producing a high magnetic field gradient would be needed for this system, and so NdFeB magnets were chosen. It was also determined that three rod-shaped magnets (3 mm diameter, 6 mm long) placed at a distance of approx. 2.5 mm from the side and staggered along the length of the separation chamber would exhibit a suitable magnetic flux density and field strength of 130 mT. Furthermore, the magnetic field gradient (as a gross linear approximation) amounted to roughly 50 mT mm^{-1}. The positioning of the magnets was selected by an educated guess initially and then further optimized empirically.

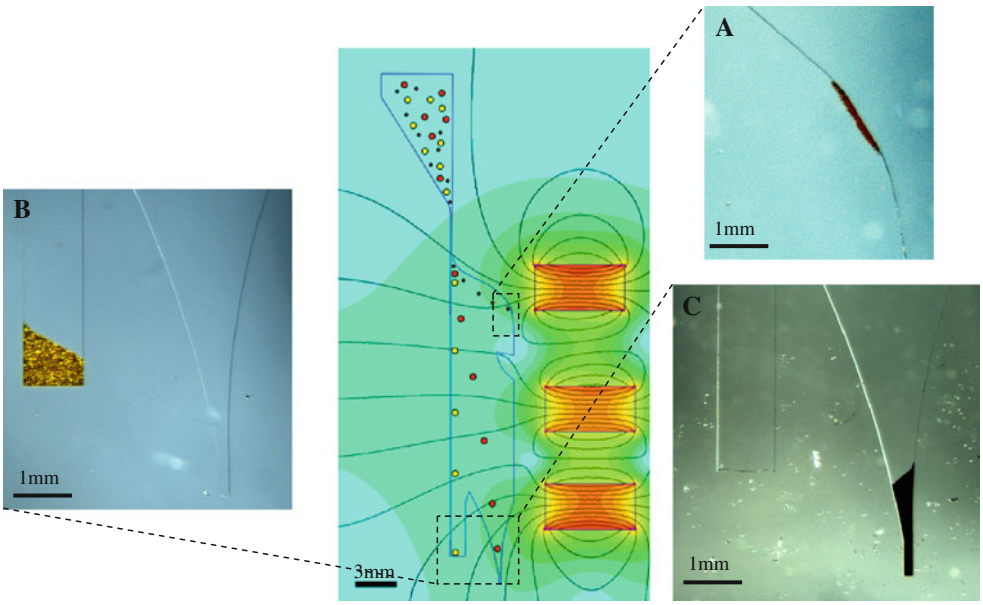

Fig. 3 Images of captured particles from three separate experiments. Capture area **a** 1-μm magnetic beads were deflected strongly due to their slow sedimentation speed and 100 % trapping was observed. Capture area **b** 100 % of the 20-μm non-magnetic beads were recovered. Capture area **c** All 20-μm magnetic particles were retrieved

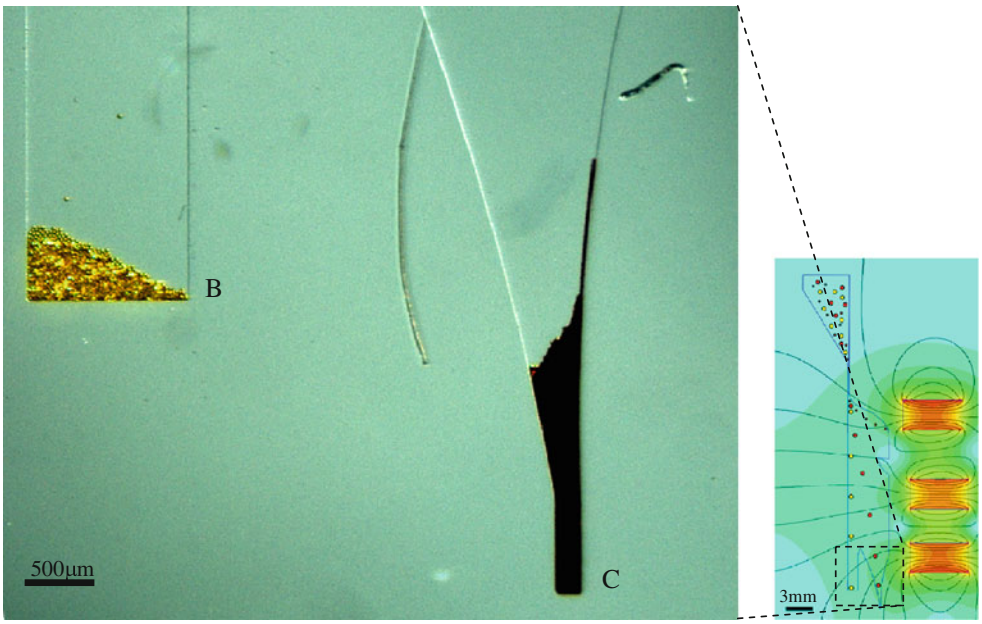

Fig. 4 After introduction of a mixture of yellow, 20-µm nonmagnetic beads and red, 20-µm magnetic beads into the loading chamber, the system was spun at 420 RPM. A complete, 100 % separation of the beads was observed

To validate the simulation results, the magnetic field was also measured using a Gaussmeter (#CYHT201, Chen Yang Technologies, DE). We measured a magnetic field strength of 100 mT (±10 %) and a magnetic field gradient (again as a gross linear approximation) of 30 mT mm^{-1}, correlating well with the modeled data.

3 Results and discussion

This work focuses on the general introduction of the fundamental concept of centrifugo-magnetophoretic separation. A preliminarily optimized, fixed magneto-microfluidic system configuration was chosen from a wide range of possible layouts to demonstrate various basic functional modes of the system. Experimental results from the solely particle-based experiments are first presented, showcasing magnetophoretic separation capabilities of our novel system along with considerations of the relative forces involved. Finally, the results of biomimetic experiments are highlighted, showing the high potential for real-world applications (Fig. 4).

3.1 Particle-based results and discussion

We start this section with a brief description of the forces present in this system to leverage the interpretation of the subsequently presented experimental results and functional modes.

3.1.1 Separation forces

Particle motion in the system is governed primarily by the centrifugal (f_ω) and magnetic (f_M) forces, and to a smaller extent by the velocity-dependent Stokes drag (f_D). At elevated particle speeds (relative to the disc), the rotational Coriolis force (f_C) also plays a role in the particle routing mechanism (Brenner et al. 2005). Briefly, the Coriolis force, which acts in the same plane as the disc, forces particles in a direction perpendicular to that of the centrifugal force and opposite to that of the direction of rotation. In fact, for a sufficient magnitude at high sedimentation speeds, the Coriolis force may artificially enhance or counteract the observed magnetic deflection/routing.

The relative strengths of the forces acting on a single magnetic particle can be estimated based on known and observed characteristics of the platform in combination with the results obtained from the magnetic modeling and measurements. The following equations describe the magnitudes of the four forces present in the system:

$$|f_\omega| = m\,d\,\omega^2 \tag{1}$$

$$|f_M| = \frac{|\chi_P - \chi_M| \cdot V_P}{\mu_0} |(\vec{B} \cdot \nabla)\vec{B}| \tag{2}$$

$$|f_D| = 6\,\pi\,\eta\,r_0\,v \tag{3}$$

$$|f_C| = 2\,m\omega\,v \tag{4}$$

where m is mass of the particle, d its distance from the particle center to the center of the disc, ω is the angular frequency of the disc rotation, χ_P and χ_M are the magnetic (volume) susceptibilities of the particle and the medium, respectively, V_P is the volume of the particle, B is the magnetic flux density that arises from the on-chip permanent magnet, μ_0 is the vacuum permeability constant (1.2566×10^{-6} V s A^{-1} m^{-1}), η is the viscosity of the carrier fluid, r_0 is the radius of the particle, and v is the velocity of the particle (Ducrée et al. 2007; Pamme and Manz 2004).

For the purposes of these calculations, a 20-μm magnetic particle with a density of 1.9 g cm^{-3} is located at the side of the separation chamber closest to and radially aligned with the magnet (at a distance from the center of rotation of about 35 mm). It is worth noting that a particle at this position experiences a maximum magnetic force, and a measured magnetic flux density in the order of 100 mT with an approximate linear gradient of around 30 mT mm^{-1} was used for the calculations. The magnetic (volume) susceptibility of the particle is assumed to be on the order of 0.15 (dimensionless) based on previous publications, and water is the carrier fluid (Pamme and Manz 2004). At a spin speed of 420 RPM, a mean particle sedimentation velocity of 137 ± 12.6 μm s^{-1} was experimentally observed using "Tracker" video analysis and modeling software (http://www.cabrillo.edu/~dbrown/tracker/) over four experiments.

Based on these assumptions, an estimation of the strength of the forces acting on a single magnetic particle is obtained as follows: $f_M = 1{,}500$ pN, $f_\omega = 480$ pN, $f_D = 26$ pN, and $f_C = 0.09$ pN. Thus, the predominant forces are the magnetic f_M and the centrifugal f_ω forces, while the Stokes drag f_D and Coriolis f_C forces are less prevalent. To better understand the increased ratio between the two dominant forces ($f_M/f_\omega = 3.1$) in view of the rather moderate deflection angles observed, one must consider the transient nature of the magnetic force as experienced by the particle. While the centrifugal force is unidirectional and high in magnitude along the entire radial length of the separation chamber (about 20 mm), the particle experiences strong, lateral magnetic-force components only when in close proximity to the magnet; this strong magnetic force is thus experienced throughout a radial travel distance roughly corresponding to the width of the permanent magnets (3 mm). These crude approximations provide a 3.1-fold higher magnitude and a 6.7-fold reduced interaction interval of the magnetic force with respect to the centrifugal force. Thus, it can be concluded that in the time-average over the two forces, their effective impact on the particle trajectory is comparable and can, therefore, be utilized to fine-tune the routing of magnetic particles through the separation chamber.

3.1.2 *Separation of magnetic from non-magnetic particles*

The fundamental capability of centrifugo-magnetic separation is first demonstrated in its most simple variant, the capture of 20-μm non-magnetic beads, 20-μm magnetic beads and 1-μm magnetic beads in three separate capture areas at a spin rate of 420 RPM (Fig. 3). The selective routing of the beads to designated capture zones roots in the specific interplay of the centrifugal force f_ω (1), magnetic force f_M (2) and the Stokes drag f_D (3). The non-magnetic particles simple follow f_ω to sediment straight down the channel. The 20-μm magnetic beads are additionally impacted by f_M to laterally deflect them into capture area C. And finally, the 1-μm magnetic beads are much lighter than the 20-μm beads; therefore, they move slowly through the centrifugal field f_ω, thus experiencing a greater deflection by the lateral magnetic field f_M into the capture area A (Fig. 3).

The next stage was the separation of magnetic from non-magnetic particles. To this end, a mixture of magnetic and non-magnetic polystyrene particles of similar size (~20 μm in diameter) was processed at a low spin speed of 420 RPM for about 20 min. The results in Fig. 4 feature an excellent degree of accuracy and exhibit 100 %

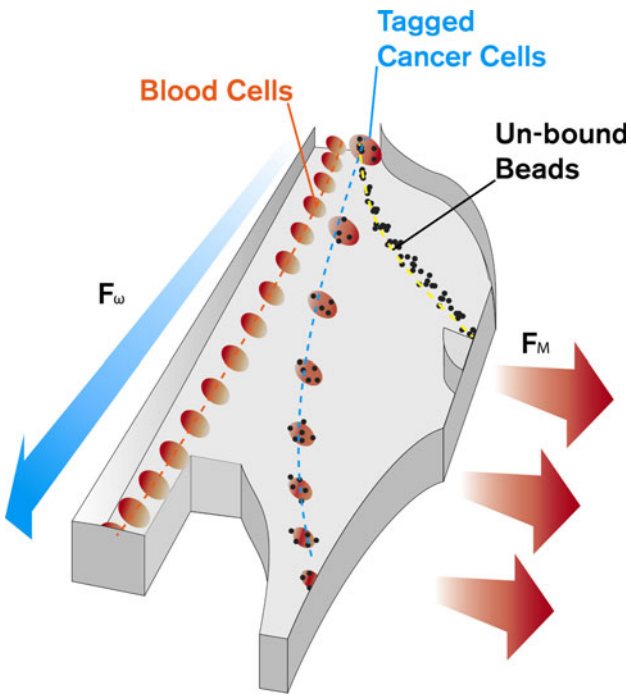

Fig. 5 Schematic of the centrifugo-magnetic principle as applied to separating magnetically tagged cancer cells from a background of healthy blood cells and excess tagging beads. The principle is the same as the bead separation and shows great promise as a method of separating cells, e.g., CTCs from a background of healthy cells (color figure online)

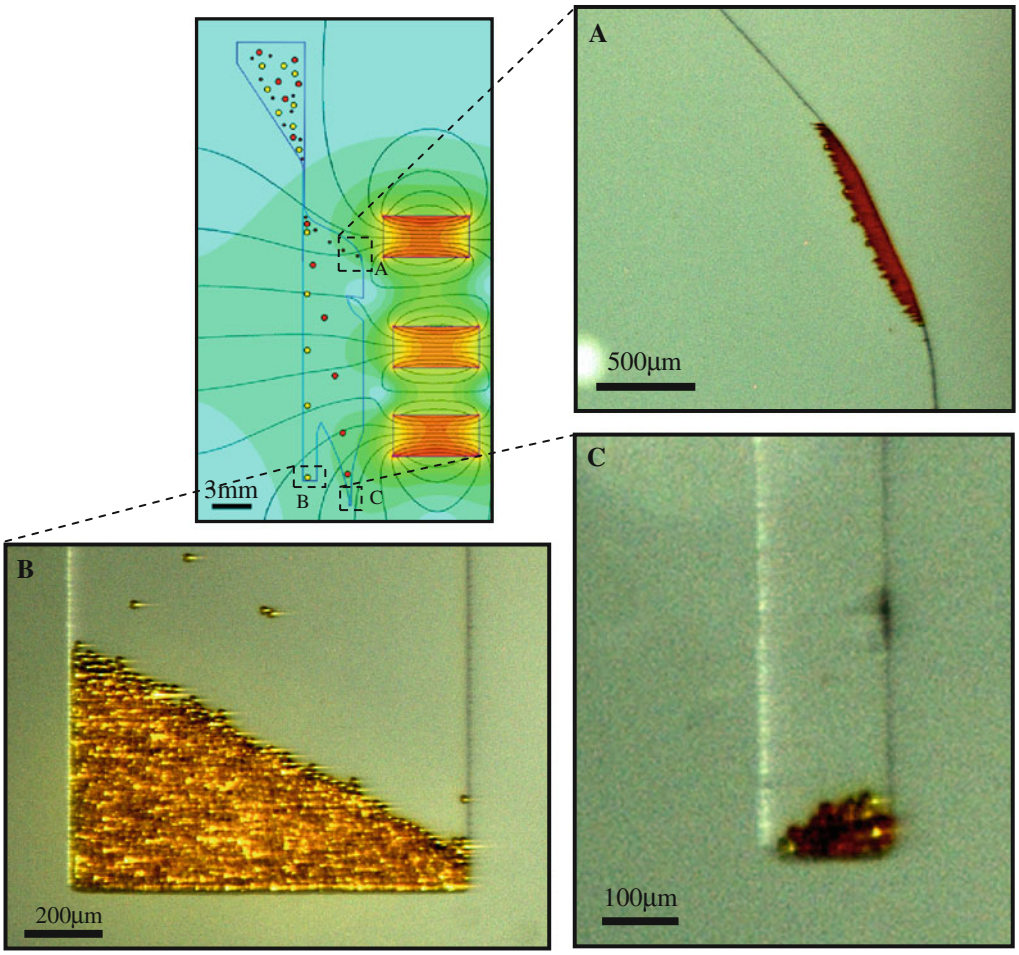

Statistical data from five runs of 3-way particle separation			
Capture area	**20 µm non-magnetic**	**20 µm magnetic**	**1 µm magnetic**
A	3 (0.02%)	0 (0%)	$7.1x10^5$ (100%)
B	16,344 (99.93%)	1.4 (3.7%)	0 (0%)
C	9 (0.05%)	36 (96.3%)	0 (0%)

Fig. 6 Results of biomimetic experiments with a large concentration of 20-µm *yellow* non-magnetic beads and *red* 1-µm magnetic beads representing healthy cells and tagging particles, respectively and a very low concentration of red 20-µm magnetic beads representing tagged cancer cells. The position of the images (taken from one of the five runs) is indicated on the schematic. The separation was done with a very high affinity, very close to 100 %. Statistical results from the five runs can be seen in the table above which indicates the average number of each particle captured in each area. Percentage values are also given. The fact that this level of separation can be achieved from a mixed population of three samples shows great promise for applying this system to separate cells (color figure online)

separation of 20-µm non-magnetic from 20-µm magnetic beads.

The next mixture of particles separated was 20-µm non-magnetic beads and 1-µm magnetic beads. Both types of beads followed the same pathway as they did when run separately through the system (Fig. 3) with 100 % of non-magnetic 20-µm beads captured ending up in capture area B and 100 % of 1-µm magnetic beads captured ending up in capture area A. The initial branching of the bead trajectories upon entering the separation chamber in Fig. 1c shows the 1-µm beads forming "trains" of beads as they line up along the magnetic field lines (Melle et al. 2001) and deflecting to the right-hand magnets, with the 20-µm non-magnetic beads continuing radially outwards.

It should be mentioned that the Coriolis force f_C (4) may to a small extent artificially enhance the observed magnetic

separation. However, we selected the rotation such that f_C counteracts f_M, thus preventing an enhancement of the lateral deflection. So the experimental results obtained on the presented choice of the centrifugo-magnetophoretic system design with the specified control parameters provide clear evidence for capability of particle focusing and separation.

3.2 Biomimetic separation results and discussion

The final set of experiments was performed to mimic the realistic conditions of extremely rare CTCs suspended in the blood stream. Typically, one CTC would be present in a background of around 1,000,000 blood cells. Our biomimetic sample consisted of a very high concentration of 20-μm polystyrene beads ("main blood cells") spiked with a minute concentration of 20-μm magnetic beads ("magnetically tagged rare cells") and a high concentration of 1-μm beads ("excess, i.e., unbound magnetic tagging beads"). Note that at this pioneering stage of our research, the CTC-to-blood-cell ratio chosen is still significantly higher in our biomimetic sample than in a patient blood to avoid problems with the otherwise required handling of large-scale, milliliter volumes on miniaturized lab-on-a-chip system. The final test consisted of five runs with an average content per run of ~16,300 non-magnetic beads (20-μm, i.e., mimicking non-target cells), ~37 magnetic beads (20 μm, i.e., mimicking tagged target cells) and ~700,000 magnetic tagging beads (1 μm, i.e., mimicking unbound magnetic tags).

These samples were separated with extremely high selectivity (Fig. 6). It was observed over the five runs that 96.3 ± 11.2 % of the 20-μm magnetic particles (representing CTCs) were captured in the correct terminus C, there were only a small fraction (3.7 %) of false negatives ("CTCs in B") and <0.1 % false positives ("regular blood cells in C"). While this level of error is very small, it would be an unacceptable amount of error if the system were scaled up to handle realistic CTC concentrations. The reason for the error was observed to be non-specific binding of a non-magnetic bead ("regular blood cell") to a magnetic tagging bead and its resulting routing into chamber C. This issue may possibly be resolved by suitable optimization of bioanalytical immuno-binding and blocking strategies.

4 Conclusions and outlook

In this work, a novel centrifugo-magnetophoretic platform for particle separation was conceptually introduced and experimentally investigated. According to their physical properties, such as size and magnetization, the distribution of the magnetic field, and the freely programmable spin speed, the platform is capable of routing microparticles into one out of three available outlets. For a chosen system configuration, a set of basic functional modes was investigated using a range of particle types and rotational frequencies. In this proof-of-concept study, prospective cell separation capability was evaluated by biomimetic experiments utilizing particles of similar mass, size and magnetization as target and background cells as well as an abundance of 1-μm magnetic tagging particles. The main advantages of the simple and robust platform are the very stable hydrodynamic conditions in the centrifugally enabled, jitter-free, stopped-flow mode which is unique to the centrifugal platform. In the future, even multidimensional cell separation may be enabled.

As established in the literature, the centrifugal microfluidic platform is also well-amenable for powerful sample preparation, including classic methods such as blood separation through centrifugation (Cho et al. 2007; Ducrée et al. 2007; Gorkin et al. 2010; Haeberle et al. 2006; Haeberle and Zengerle 2007; Madou et al. 2006; Steigert et al. 2007a, b). This suggests great opportunity towards a full-fledged, high-performance sample-to-answer system for a wide spectrum of applications involving a cell separation function.

Acknowledgments This work was supported by the Science Foundation of Ireland under Grant No. 10/CE/B1821.

References

Beebe D, Mensing G, Walker G (2002) Physics and applications of microfluidics in biology. Annu Rev Biomed Eng 4:261–286

Brenner T, Glatzel T, Zengerle T, Ducrée J (2005) Frequency-dependent transversal flow control in centrifugal microfluidics. Lab Chip 5:146–150

Burger R, Ducrée J (2012) Handling and analysis of cells and bioparticles on centrifugal microfluidic platforms. Expert Rev Mol Diagn 12(4):407–421. doi:10.1586/ERM.12.28 (in press)

Cho Y, Lee J, Park J, Lee B, Lee Y, Ko C (2007) One-step pathogen specific DNA extraction from whole blood on a centrifugal microfluidic device. Lab Chip 7:565–573

Ducrée J, Haeberle S, Lutz S, Pausch S, von Stetten F, Zengerle R (2007) The centrifugal microfluidic bio-disk platform. J Micromech Microeng 17:103–115

Finite Element Method Magnetics (FEMM) http://www.femm.info. Accessed Jul 2010

Gijs M (2004) Magnetic bead handling on-chip: new opportunities for analytical applications. Microfluid Nanofluid 1:22–40

Gorkin R, Park J, Siegrist J, Amasia M, Lee B, Park J, Kim J, Kim H, Madou M, Cho Y (2010) Centrifugal microfluidics for biomedical applications. Lab Chip 10:1758–1773

Grumann M, Brenner T, Beer C, Zengerle R, Ducrée J (2005) Visualization of flow patterning in high-speed centrifugal microfluidics. Rev Sci Instrum 76:025101

Haeberle S, Zengerle R (2007) Microfluidic platforms for lab-on-a-chip applications. Lab Chip 7:1094–1110

Haeberle S, Brenner T, Zengerle R, Ducrée J (2006) Centrifugal extraction of plasma from whole blood on a rotating disk. Lab Chip 6:776–781

Hosokawa K, Sato K, Ichikawa N, Maeda M (2004) Power-free poly(dimethylsiloxane) microfluidic devices for gold nanoparticle-based DNA analysis. Lab Chip 4:181–185

Karle M, Miwa J, Czilwik G, Auwärter V, Roth G, Zengerle R, von Stetten F (2010) Continuous microfluidic DNA extraction using phase-transfer. Lab Chip 10:3284–3290

Madou M (2002) Fundamentals of microfabrication, 2nd edn. CRC Press, Boca Raton

Madou M, Zoval J, Jia G, Kido H, Kim J, Kim N (2006) Lab on a CD. Annu Rev Biomed Eng 8:601–628

Manz A, Graber N, Widmer H (1990) Miniaturized total chemical analysis systems: a novel concept for chemical sensing. Sens Actuators B 1:244–248

Melle S, Rubio M, Fuller G (2001) Time scaling regimes in aggregation of magnetic dipolar particles: scattering dichroism results. Phys Rev Lett 87:115501

Pamme N (2006) Magnetism and microfluidics. Lab Chip 6:24–38

Pamme N (2007) Critical review: continuous flow separations in microfluidic devices. Lab Chip 7:1644–1659

Pamme N, Manz A (2004) On-chip free-flow magnetophoresis: continuous flow separation of magnetic particles and agglomerates. Anal Chem 76:7250–7256

Pamme N, Wilhelm C (2006) Continuous sorting of magnetic cells via on-chip free-flow magnetophoresis. Lab Chip 6:974–980

Pappas D, Wang K (2007) Cellular separations: a review of new challenges in analytical chemistry. Anal Chim Acta 1:26–35

Siegrist J, Peytavi R, Bergeron M, Madou M (2009) Microfluidics for IVD analysis: triumphs and hurdles of centrifugal platforms—Part 1: molecular fundamentals. IVD Tech 15:22–26

Silbert L (2010) Jamming of frictional spheres and random loose packing. Soft Matter 6:2918–2924

Steigert J, Brenner T, Grumann M, Riegger L, Lutz S, Zengerle R, Ducrée J (2007a) Integrated siphon-based metering and sedimentation of whole blood on a hydrophilic lab-on-a-disk. Biomed Microdevices 9:675–679

Steigert J, Haeberle S, Müller C, Steinert CP, Gottschlich N, Reinecke H, Rühe J, Zengerle R, Ducrée J (2007b) Rapid prototyping of microfluidic chips in COC. J Micromech Microeng 17(2): 333–341

ThermoScientific KingFisher http://www.thermoscientific.com/wps/portal/ts/products/detail?productId=11960640. Accessed Nov 2010

Thorsen T, Maerkl S, Quake S (2002) Microfluidic large-scale integration. Science 298:580–584

Veridex http://www.veridex.com. Accessed Oct 2010

Xia Y, Whitesides G (1998) Soft lithography. Annu Rev Mat Sci 28:153–184